Reliable Inkjet-Printed Interconnections on Foil-Type Li-Ion Batteries

N. B. Palacios-Aguilera, H. A. Visser, Ashok Sridhar, Unai Balda-Irurzun, Laura D. Vargas-Llona, Jiang Zhou, Remko Akkerman, P. J. French, and Andre Bossche

***Abstract*—Shapeable rechargeable Li-ion batteries are a good option for the power source of system-in-package devices; nevertheless, their size and temperature limitations are a constraint during the fabrication process. Inkjet-printed interconnections on top of the battery are proposed in order to reduce the size and costs of wireless sensor network devices that require the use of Li-ion batteries. The reliability of such interconnections under high-humidity and elevated-temperature conditions is characterized in terms of electrical and adhesion properties; the micro- and macrostructures of the ink are observed in detail. Two silver inks are used to print the interconnections. The resistivity values of printed structures are in the range of 8.6–47.6 $\mu\Omega \cdot$ cm, and all of them pass the reliability tests. The adhesion characteristics are good for Ink A; however, Ink B presents failures under high-humidity conditions. For a good adhesion, a plasma treatment should be performed prior to printing. The electrical performance of the interconnections is not affected by high-humidity and high-temperature conditions. Furthermore, there is no indication of silver migration. It is recommended that the curing temperature of the ink is kept low ($< 155\ ^\circ$C) in order to avoid cracks in the ink structure and damages to the battery's packaging foil. The interconnections should be printed before filling the battery to avoid the decomposition of the electrolyte which happens at 80 °C.**

***Index Terms*—Adhesion, inkjet printing, Li-ion battery, nanoparticle inks, reliability, resistivity, system in package (SiP).**

I. Introduction

In THE coming years Wireless Sensor Networks (WSNs) and active tag technologies are envisaged to usher new concepts in logistics and asset management. It is the vision of the PLEISTER (Packaged Label Electronics Including Sensing Talkative Enhanced Radio) project, funded by the Dutch Technology Foundation (STW), that a group of designated active tags can jointly form a self-contained ad hoc network capable of monitoring itself. Joining or leaving the group will be noticed immediately and reported to external entities. Moreover, status information such as location, temperature, humidity, among others will be sensed and monitored. An active tag must therefore have at least the following elements: antenna, battery, small embedded systems, and sensors; such elements will be integrated as a system in package (SiP).

Within the framework of the PLEISTER project, the System-in-Package approach presents the following challenges and constraints for each active tag: it must be cheap using economic materials like foils as substrates instead of silicon or ceramics, it must have a total maximum size of 2 cm $\times$ 2 cm $\times$ 1 cm, the operation frequency is 2.4 GHz and it has to be compliant with RoHS regulations. Moreover, the package design must provide an environmental opening for different kinds of sensors thus providing a flexible platform that allows the use of any sensor, including the ones that require direct contact with the environment. The battery to be used for the SiP is a shapeable Li-ion battery under research and development by Philips.

A. Proposed System Architecture

Since the Li-ion battery is the largest and mechanically most stable component in the node, it is proposed to use it as the substrate for the whole SiP. Silver ink inkjet-printed interconnection circuits are an option to reduce and optimize space, materials and costs of the package, since material is deposited only where it is needed.

Fig. 1 shows the SiP concept. The goal is to use the shapeable Li-ion battery as substrate by printing the interconnection lines directly on top of it.

The adhesion between the battery package and the printed silver ink should be optimized to fabricate reliable circuit interconnections; this particular aspect is dealt with in detail in this paper as well as the study of the reliability and performance of such printed interconnection lines with supporting experiments, which include adhesion testing and electrical characterization.

B. Incorporating the Li-ion Battery Into the SiP: Constraints

Shapeable Li-ion batteries have been in research and development in the last decade and are currently available to the market; nevertheless some challenges and/or constraints, which are enlisted in this section, have to be overcome in order to incorporate them into SiPs.

Fig. 2(a) shows the cross-section of the foil that forms the package for such batteries, which has a 25 μm thick

Manuscript received February 1, 2012; revised September 10, 2012 and September 25, 2012; accepted October 2, 2012. Date of publication October 10, 2012; date of current version March 7, 2013. This work was supported in part by the Dutch Technology Foundation (STW).

N. B. Palacios-Aguilera, P. J. French, and A. Bossche are with Delft University of Technology, 2628 CN Delft, The Netherlands (e-mail: n.b.palaciosaguilera@tudelft.nl; p.j.french@tudelft.nl; a.bossche@tudelft.nl).

H. A. Visser, L. D. Vargas-Llona, and R. Akkerman are with the University of Twente, 7500 AE Enschede, The Netherlands (e-mail: H.A.Visser@utwente.nl; L.D.Vargas@utwente.nl; R.Akkerman@utwente.nl).

A. Sridhar was with the University of Twente, 7500 AE Enschede, The Netherlands. He is now with TNO/Holst Centre, 5656 AE Eindhoven, The Netherlands (e-mail: ashok.sridhar@gmail.com).

U. Balda-Irurzun was with the University of Twente, 7500 AE Enschede, The Netherlands. He is now with Innovalia Metrology, 48008 Bilbao, Spain (e-mail: u.baldairurzun@gmail.com).

J. Zhou was with Philips Research Europe, 5656 AE Eindhoven, The Netherlands. He is now with China BAK Battery, Inc., Shenzhen 518119, China (e-mail: jzhou02@yahoo.com).

Digital Object Identifier 10.1109/TDMR.2012.2223759

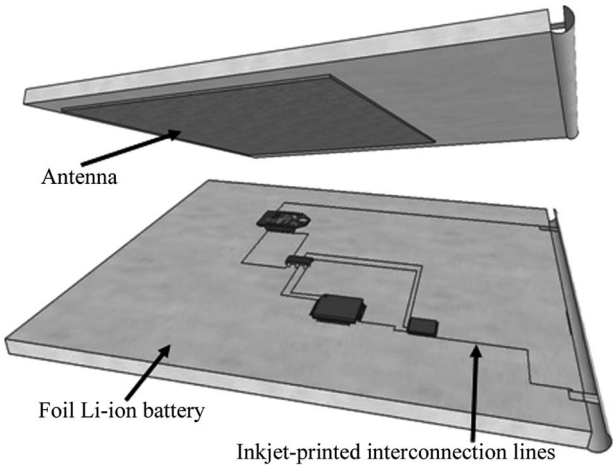

Fig. 1. Schematic of the SiP concept.

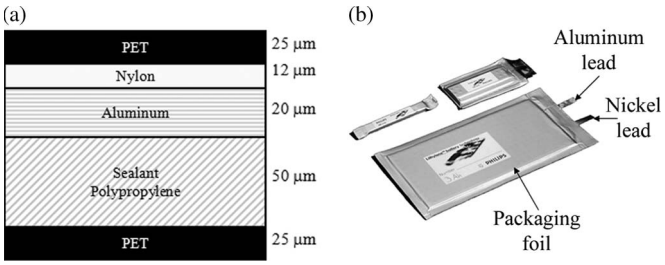

Fig. 2. Composition of the battery package foil (a) and fabricated battery (b).

polyethylene therephthalate (PET) layer at the outer surface. Fig. 2(b) shows fabricated batteries; it is possible to observe the packaging foil on which the interconnection circuits will be printed.

The melting point of the polypropylene (PP) layer in Fig. 2(a) is around 160 °C and the electrolyte of the battery starts to decompose at 80 °C [1]. As a consequence, the battery packaging foil cannot be subject to temperatures higher than 155 °C and the battery itself cannot be subject to processes at temperatures higher than 80 °C.

II. Specimen Preparation and Testing

A. Materials and Specimen Preparation Methods

A commercially available battery foil (Sumitomo Chemical Co., Ltd.) with a thickness of 132 μm described in Section I-B is used as substrate. Two different commercially available silver inks are tested.

The first ink (Ink A) used to create the test structures is a silver nanoparticle based ink with a mean nanoparticle diameter of 5 nm and a metal content of 62–67 wt%. The second ink (Ink B) is also a silver nanoparticle ink with a metal content of 20 wt%. Both inks require post-deposition heating in order to sinter the nanoparticles. Specific information about the inks as well as their producers has been consciously left out.

The samples are printed using a drop-on-demand inkjet printer (Jetlab-4 from Microfab Technologies Inc., USA). The printhead contains a piezo-actuated nozzle with a diameter of 80 μm. The substrate holder is preheated to 70 °C and maintained at that temperature while printing with Ink A; in the case of Ink B, the temperature is 65 °C. By means of preheating, the spreading of the ink on the substrate is controlled as a result of quick evaporation of the solvent present in the ink. At the same time, since the nozzle of the printhead is maintained at approximately 1 mm from the substrate, the convective heat transfer from the substrate holder results in evaporation of solvent from the ink present near the tip of the nozzle, resulting in either nozzle blockage or change in jetting behavior [2]. When choosing the substrate holder temperature settings mentioned above, this issue is taken into account; at the set temperatures, only minimal change in jetting behavior was observed.

The printing is unidirectional and the droplet spacing is slightly modified on a case-to-case basis, depending on the ink used as well as the substrate surface pre-treatment used. The pre-treatment is discussed in the next section. All the specimens consist of one layer of printed silver i.e., each specimen is printed only once and not overprinted to increase layer thickness.

Subsequent to printing, the samples are thermally sintered. The samples printed with Ink A are sintered at 210 °C for 30 minutes following the manufacturer's recommendation. It is possible to sinter the ink at a temperature of 160 °C if the curing time at this temperature is long enough. Preliminary experiments indicated, however, that it is difficult to determine whether the ink layer has achieved an acceptable level of sintering after prolonged sintering times. Therefore, it is chosen to sinter at 210 °C to ensure reproducibility and complete curing of the ink, accepting the fact that this would result in a PET foil with a PP layer that lost its sealant capabilities. For the final application this important drawback of Ink A should be taken into account, but here the main goal is to characterize and compare the reliability of the printed tracks of both inks.

The samples printed with Ink B are sintered at 125 °C for 16 hours.

B. Battery's Foil Surface Preparation for Optimized Adhesion

In general, polymers have low surface energy values [5] which results in poor wettability of the ink on the substrate; for inkjet printing applications, good wettability is desired for well defined structures.

It is well known that plasma-chemical treatments result in an increase in surface energy of polymers [5]–[9]; moreover, they provide a dry, clean, low temperature and fast processing [8]. The hydrophobic surface of PET substrates can be made hydrophilic using plasma treatment.

According to [3], the interfacial adhesion in metal–polymer systems not only depends on the wettability of the polymer, but also on the morphology. Plasma treatments enhance the mechanical interlocking between substrates and inks [3]. Oxygen (O_2) based plasma is used to improve the surface energy of PET.

The morphology of the substrate surface after different plasma treatments is studied using Atomic Force Microscopy (AFM) and White Light Interferometry (WLI) techniques. The AFM measurements are performed in an area of 50 μm $\times$ 50 μm on the surface and the sampling is performed every

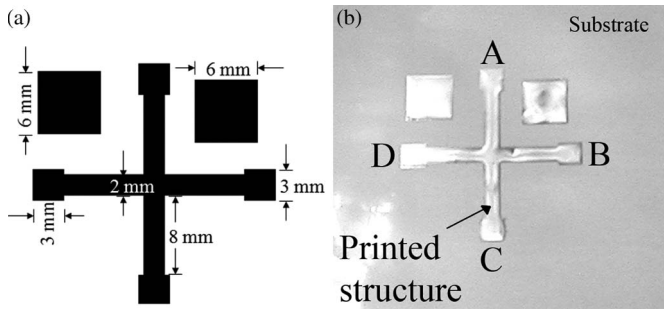

Fig. 3. Printed structure used to perform the different tests. Dimensions of the structure (a). A printed structure on the battery's packaging foil (b).

125 nm. The WLI measurements are performed in an area of 94 μm $\times$ 123 μm at a 50$\times$ magnification with a sampling distance of 168 nm. The wettability of a surface can be characterized by measuring the contact angle. The contact angle of the PET samples before and after the plasma treatment is measured using the sessile drop method in the Contact Angle System OCA 20 from Dataphysics Instruments GmbH.

Several specimens are prepared to find the plasma treatment parameters that provide the most favorable adhesion between the substrate and the ink. The treatments are performed in an Europlasma NV equipment at 100 Watts (W) for 60, 180, and 300 seconds, with an ethanol cleaning step after the treatment; specimens with the same treatments are also prepared without an ethanol cleaning step after the treatment. It is important to determine the effects of the ethanol cleaning step in the adhesion since the substrate has to be cleaned with ethanol before performing the inkjet printing process. The ethanol cleaning step consists on cleaning the surface in one direction with a tissue previously submerged in ethanol.

C. Test Methods

Adhesion tests and resistivity measurements are performed to determine the printed interconnections' performance without the influence of a bias, as well as the most suitable ink for the aimed application.

Fig. 3 shows the structure used for testing purposes. The two squares on the top of the structure are used to perform the adhesion tests and the cross structure is used to perform the resistivity measurements, which are explained later on in this section.

Furthermore, flexural testing and temperature–humidity–bias tests are performed to the chosen ink. These tests are described later in this section.

Adhesion Test Method: The adhesion test method used to identify which plasma treatment parameters provide optimal adhesion between the ink and the substrate is the Scotch-tape test [3]. This method involves the usage of a pressure-sensitive tape and provides only qualitative information about the adhesion of the coating to the substrate.

The same adhesion test method is used to test the adhesion before and after the reliability tests described later in this section.

Electrical Characterization Method: The resistivity measurements are performed using a Greek-cross structure and a 4-point configuration. The Greek cross is a common structure used to measure sheet resistance of thin films, independently of their geometry [10]–[12]. The length of the arms of the cross should be greater or equal than the size of the heart of the cross (area where arms overlap) and the sample should be homogeneous in thickness [12] to perform sheet resistance measurements using the Greek-cross configuration. Fig. 3(b) shows the printed Greek-cross structure. The Greek-cross structure allows for sheet resistance measurements with an accuracy of 0.1% in the sheet resistance [10]. A current is passed from contact A to B and voltage is measured between contacts D and C to perform the 4-point measurement. The resistance is calculated according to Ohm's law. Then, the sheet resistance R_s is obtained according to (1)[12]

$$R_s\left(\frac{\Omega}{sq}\right) = \frac{\pi R}{\ln 2}. \tag{1}$$

Taking into account the physical dimensions of the material and according to (2), the resistance is equal to the resistivity ρ multiplied by the length L and divided by the width W and the thickness t of the material, at the same time, it is also equal to the sheet resistance multiplied by the length and divided by the width of the material

$$R(\Omega) = \frac{\rho}{t}\frac{L}{W} = R_s\frac{L}{W}. \tag{2}$$

From (2), the sheet resistance is related to the resistivity via the thickness as expressed in

$$\rho(\Omega \cdot cm) = R_s \cdot t. \tag{3}$$

The thicknesses used to perform the calculations are 3 μm for Ink A and 1 μm for Ink B. The thicknesses are measured using a Dektak profiler.

A detailed discussion on the Greek-cross structure is provided in [11] and [13].

Reliability Tests: Reliability tests are performed based on the MIL-STD standards to determine whether the inkjet-printed interconnection lines on the PET foil are robust. Resistivity measurements and adhesion tests are performed on fresh samples and samples subjected to the different reliability tests. The reliability tests performed on the samples are the moisture resistance test, the thermal shock test and the temperature cycling test. The applied stresses are chosen based on the temperature range of the aimed application, previously mentioned in Section I. In addition, the temperature range is limited by the characteristics of the battery, described in Section I-B.

The moisture resistance test used is based on the MIL-STD-883C Method 1004.7. The samples are subject to 10 cycles, where the temperature is ramped from room temperature to 65 °C, then to room temperature and once more to 65 °C. The humidity level is kept between 90% RH and 100% RH. If 100% RH is used, care should be taken to avoid condensation. A low temperature step is performed during 5 of the 10 cycles at -10 °C with uncontrolled humidity. Finally, the specimens are kept at room temperature conditions for one day. Thereafter, the final measurements are performed [14].

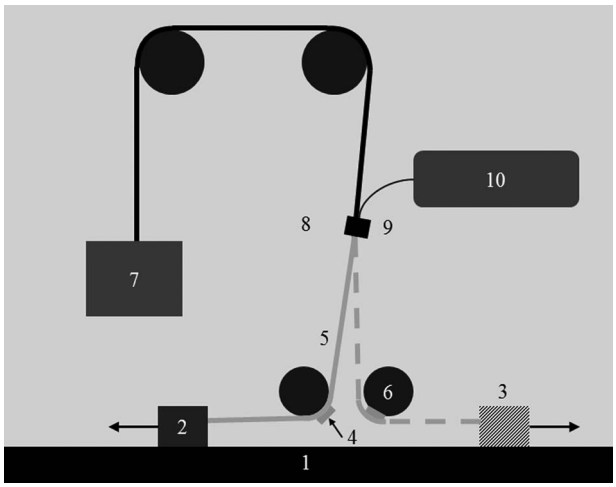

Fig. 4. Schematic of the flexural testing equipment. 1 Table. 2 Sliding clamp (end-position 1). 3 Sliding clamp (end-position 2). 4 Ultra-thin chip. 5 Flexible substrate. 6 Cylinder. 7 Counter-weight. 8 Frame. 9 Clamp/electrical connection for resistance measurement. 10 Data acquisition.

The thermal shock test performed over the specimens is based on the MIL-STD-883C Method 1011.7. The liquids used are water at 80 °C and ethanol at −20 °C. The test starts preconditioning the specimens at 80 °C for 5 minutes. Then 15 cycles are performed, where each cycle consists of keeping the samples at −20 °C for 5 minutes and then 5 minutes at 80 °C. The time when transferring the samples from high to low or low to high temperatures is less than 10 seconds.

The temperature cycling test is based on the MIL-STD-883C Notice 5 Method 1010.7. The test consists of 10 cycles, where each cycle is composed by a low temperature cycle and a high-temperature cycle at uncontrolled humidity conditions. The low temperature cycle is performed at −55 °C for 30 minutes and the high-temperature cycle is performed at 85 °C for 30 minutes. The times of the cycles consider the time indicated in the MIL-STD standard for the sample to reach the high or low temperatures, respectively.

Flexural Testing: One ink is chosen (Ink B) after determining the suitability of the inks for the intended application, by studying their qualitative adhesion and their conductivity under high-humidity and elevated-temperature conditions as well as analyzing their macro- and microstructure. Flexural testing and temperature–humidity–bias (THB) tests are performed to samples prepared with the chosen ink (Ink B). The THB test is explained later in this section.

The flexural test, in addition to determining whether the inkjet-printed interconnections withstand several flexing cycles, also gives a more realistic indication of the adhesion of the printed lines to the substrate, since flexural stresses can result in delamination.

Fig. 4 shows the flexural testing setup; the flexural tester flexes the sample both ways around a cylinder of selected radius. This setup was built in-house and can be programmed to measure the resistance using the 4-points method, after a desired number of cycles has been performed. One cycle constitutes two folding steps, one around each cylinder.

Three test specimens are prepared, each containing two lines printed with Ink B. The dimensions of each line are

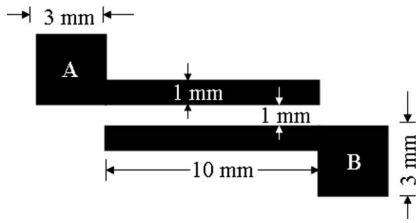

Fig. 5. Schematic of the printed samples for the THB test.

TABLE I
CONTACT ANGLE MEASUREMENTS IN DEGREES (°)

Days	No Plasma	60 s With Ethanol	180 s With Ethanol	300 s With Ethanol
0	89.4	61.8	53.4	51.0
4	90.0	67.7	59.5	57.1
15	82.3[a]	69.8	60.1	61.3
Days		60 s Without Ethanol	180 s Without Ethanol	300 s Without Ethanol
0		35.4	33.5	24.3
4		43.5	49.9	34.9
15		57.3	51.8	47.5

[a] This is an unexpected result for which we don't have an explanation.

100 mm × 0.8 mm × 1 μm. The length of 100 mm is chosen, as the stroke length of the flexural testing equipment is set at 80 mm. The electrical resistance of the individual lines on the specimens is measured at the start and at the end of the test. The number of cycles is chosen as 1000 cycles and the radius of the cylinder as 10 mm, both values being fairly representative of practical applications, as well as adopted by similar published research [15].

Temperature–Humidity–Bias Test: The purpose of the THB test is to determine the silver migration as well as expected use lifetime. The THB test is based in the standard test method for silver migration from ASTM, designation F 1996-06.

The specimens are stabilized at room temperature conditions (21 °C–25 °C/50% RH) for 24 hours. Subsequently, the initial insulation resistance is measured and the power supply is connected. The voltage applied is 5 V and the current is limited to 2 mA. The different temperature–humidity conditions are applied: (a) 85 °C/85% RH and (b) 125 °C/85% RH. After 10 days, the power supply is disconnected and the samples are stabilized at room temperature conditions as at the beginning of the test. The final insulation resistance is measured. Furthermore, the samples are visually inspected before and after the test. The samples are inspected at a maximum magnification of 20× under the microscope for dendrite formation.

Fig. 5 shows the test specimen. Six specimens are printed with Ink B per test condition. The printing and sintering process is carried out as explained in Section II-A. The selected size of the test pattern is based on the IPC standard SM-840.

Since there were no failures in the specimens printed according to Fig. 5, an extra set of 6 specimens is printed for condition (b) to find any failure. The space between lines is 260 μm and the width of the lines is 110 μm instead of 1 mm. These samples are printed pushing to the limits of the 80 μm nozzle, that is to say, the smallest line and space between lines possible with

TABLE II
AVERAGE ROUGHNESS OF PET SAMPLES AFTER DIFFERENT PLASMA TREATMENTS

Plasma treatment duration (s)	0	60	180	300
WLI measured roughness (nm)	45.6	48.3[a]	50.5[a]	40.9[a]
WLI measured roughness (nm)	45.6	51.1[b]	54.4[b]	45.0[b]
AFM measured roughness (nm)	14.8[a]	22.6[a]	26.8[a]	18.2[a]

[a] Samples with ethanol cleaning step after plasma treatment.
[b] Samples without ethanol cleaning step after plasma treatment.

printing-on-the-fly activated; printing-off-the-fly can result in even thinner lines. The size of the test pattern in this case is selected based on the JPCA standard BU01 for fine patterns.

III. RESULTS AND DISCUSSION

A. Optimized Adhesion

The adhesion of the PET surface has to be optimized as explained in Section II-B. Table I shows contact angle measurements immediately after the plasma treatment and after 4 and 15 days. Some samples are cleaned with ethanol after the plasma treatment. The angles measured immediately after the plasma treatment are comparable to the ones reported by [6] and [16]. The liquid used to measure the contact angle is deionized water and the values represent the average of 5 measurements performed on different locations on the specimen surface.

The results in Table I show that ethanol increases the contact angle of the PET, achieving surface energy stabilization in a shorter period of time. The contact angle of the samples cleaned with ethanol after the plasma treatment increases less than 10° in 15 days while the contact angle of the samples that are not cleaned increases more than 20° in 15 days. This difference affects the shelf life of the samples between the plasma treatment and the printing process, affecting the wettability of the substrate and therefore the spreading of the ink.

Table II shows the average roughness measured with AFM and WLI. The O_2 plasma treatment causes a maximum of the average roughness at 180 seconds. The ethanol cleaning step after the plasma treatment does not affect the roughness much. Plasma treatment etches the surface, if the surface is subject to plasma treatment for a longer time than necessary the residuals may stay on the surface, causing a decrease in the average roughness. Since adhesion not only depends on surface energy but also on mechanical interlocking, even if the contact angle is less, it does not imply that the adhesion is better. As observed from Table II, the average roughness can start to decrease at a determined plasma treatment duration, affecting the adhesion results in a negative way.

Furthermore, the measurements between AFM and WLI techniques differ due to the scanned area size. If a smaller area is scanned, for instance 40 μm $\times$ 40 μm; the average roughness could be as low as 15 nm since there is a bigger chance of not including the random bumps in the measured area. As a conclusion from these measurements, WLI is a more appropriate technique to measure the surface average roughness due to the fact that it allows scanning much larger areas than AFM. The problems associated with WLI can be overcome by carefully focusing the equipment.

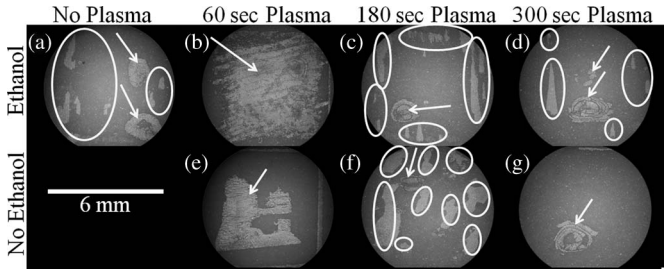

Fig. 6. Scotch-tape adhesion test results for Ink A as a function of ethanol cleaning and plasma treatment. Circles show adhesion failure occurring in the tape (desirable), and arrows show adhesion failure occurring in the ink (undesirable).

TABLE III
SUMMARY OF DIFFERENT PLASMA TREATMENTS TESTS AND MEASUREMENTS

Plasma treatment duration at 100 W (s)	Contact Angle (°)	Contact Angle Variation (°)	Roughness (nm)	Adhesion (ranking)
No plasma	89	-	45.6	2
60[a]	61	8.0	48.3	1
60[b]	35	21.9	51.1	1
180[a]	53	6.7	50.5	4
180[b]	33	18.3	54.4	4
300[a]	51	10.3	40.9	3
300[b]	24	23.2	44.9	3

[a] Samples with ethanol cleaning step after plasma treatment.
[b] Samples without ethanol cleaning step after plasma treatment.

The results reported by [16] differ from the results reported here in magnitude; nevertheless, they are measured using AFM in a 5 μm $\times$ 5 μm area.

Fig. 6 shows the results of the adhesion test, in other words, the Scotch tape that is attached to and subsequently peeled off from the inkjet-printed structures. The circles surround the adhesion failures of the Scotch tape adhesive, that is to say, the Scotch tape adhesive is adhered to the printed ink structure failing before the printed structure fails. The arrows point at the failures of the silver layer printed on PET, that is to say, silver ink that was adhered to the Scotch tape after peeling this last one off from the test specimen. The treatment of 180 s provides the best adhesion characteristics because of the big amount of failures from the tape but the low amount of failures from the ink.

The ink used in this experiment is Ink A. The adhesion of Ink B is not tested here since the purpose of the experiments in this section is to identify general plasma treatment parameters that allow the PET surface achieve the surface characteristics that encourage the most favorable adhesion characteristics.

Table III shows a summary of the tests and measurements results for the different plasma treatment specimens. The contact angle column indicates the contact angle of a water drop on PET, the higher the number the higher the contact angle and thus the more hydrophobic the surface is. The number in the contact angle column represents the average of the measured contact angles immediately after the plasma treatments are

TABLE IV
AVERAGE RESISTIVITY IN $\mu\Omega \cdot$ cm FOR THE DIFFERENT AGING PROCESSES AND FRESH SAMPLES

	Ink A		Ink B	
	Fresh Sample	Tested Sample	Fresh Sample	Tested Sample
Thermal Shock	15.8	16.8	15.7	14.4
Moisture Resistance	31.1	31.1	12.3	10.6
Temperature Cycling	28.6	28.1	14.9	14.6

TABLE V
PERCENTAGE OF RESISTIVITY CHANGE AFTER THE AGING PROCESS WITH RESPECT TO THE FRESH SAMPLE

	Ink A	Ink B
Thermal Shock	6.9	-8.1
Moisture Resistance	-2.2	-14.2
Temperature Cycling	-2.1	-1.6

performed. The contact angle variation column gives the increase of contact angle 15 days after performing the surface treatment. The roughness column indicates the average roughness of the surface in nanometers. The adhesion column expresses qualitatively how good the adhesion between the ink and the PET surface is, the better the adhesion the higher the value; these values are assigned by making a visual comparison between all the samples.

The plasma treatment that provides the best characteristics to achieve the most favorable interface adhesion is 180 s at 100 W. The combination of contact angle and roughness characteristics provided by such treatment promotes the best adhesion characteristics, cleaning the samples with ethanol after the plasma treatment does not affect the adhesion properties.

The optimal plasma treatment chosen to treat the battery foil prior to print the interconnections is 180 s at 100 W with an ethanol cleaning step after the plasma treatment. The ethanol cleaning step is chosen because the samples need to be cleaned prior to printing. The samples used for the reliability and performance tests are prepared using such surface preparation process.

B. Reliability of Printed Interconnections

Electrical Performance: Table IV shows the results of resistivity in $\mu\Omega \cdot$ cm for the different aging processes as well as the fresh samples. The numbers represent the average resistivity of three specimens for each tested condition.

Table V shows the average percentage of resistivity change after the aging processes with respect to the fresh samples; the percentage is not obtained directly from the average resistivity in Table IV, it is the average of the percentages calculated by separate. A negative sign indicates a decrease of resistivity in relation to the fresh sample resistivity. The samples that present a change in resistivity after the reliability tests lower than 20% can be considered a pass according to industry standards [17] and literature [18]. A decrease on the resistivity is favorable, as specified also in literature [18].

Furthermore, the fresh specimens of Ink A present a standard deviation of 13.95 and the ones of Ink B present a standard deviation of 3.32.

All the samples are considered as pass since the percentage of change in the resistivity value is less than 20% in all the cases, the increases/decreases in the values are due to the aging processes the samples are subject to. Furthermore, the silver ink resistivity values obtained are at least 6 times higher than bulk silver resistivity; the pure silver resistivity is 1.59 $\mu\Omega \cdot$ cm.

Ink B proves to obtain more reproducible results, nevertheless, the variations observed in the resistivity values are due to human and environment variations. The equipment used during the experiments is for research purposes and can be expected to result in a lower reproducibility than one designed for production.

Adhesion: The adhesion of both inks before and after the aging processes is studied following the same procedure explained in Section II-C.

Fig. 7 shows the Scotch tape that is attached to and subsequently peeled off from the inkjet-printed structures. It is possible to observe that Ink A is more resistant to the aging processes in terms of adhesion. Ink B presents perfect adhesion characteristics prior to the reliability tests; nevertheless, after being subject to the aging processes, Ink B presents a considerable amount of failures. Further tests are proposed to investigate and improve the adhesion of Ink B.

Micro- and Macrostructure: Concerning the macrostructure of the inks, Ink A exhibits cracks after curing presumably due to the high curing temperatures and the Coefficient of Thermal Expansion (CTE) difference between the PET and the ink. Fig. 8(a) shows the center of a structure printed with Ink A, the circle indicates the crack; similar cracks appear in all the specimens printed with Ink A. Fig. 8(b) shows the center of a structure printed with Ink B; for this ink no cracks are present in any of the specimens due to the lower curing temperature.

Fig. 9 shows the microstructure of the inks with a magnification of 5000×. Fig. 9 shows that the samples printed with Ink A present some clear boundaries formed due to the CTEs mismatch of the PET foil and the ink itself, and the high curing temperatures. The grainy structure observed on the moisture resistance (Ink A) sample is artifact from the SEM equipment used to scan the specimen. Concerning the samples of Ink B, it is possible to observe that the grainy structure is consistent even if the samples are subject to different aging processes; the ink microstructure is not affected by high-temperature and/or high-humidity conditions.

Flexural Testing: All the 6 printed lines pass the flexural testing without any significant change in electrical resistance. The average measured resistance before the test is 144.5 Ω and after the test is 146.3 Ω, an average increase of 1.24%. This demonstrates that there is no significant crack formation in the printed lines. Microscopic analysis also shows that there is no delamination of the printed lines.

Temperature–Humidity–Bias Test: All the 6 specimens for each test condition present an initial insulation resistance between 6×10^9 Ω and 1.2×10^{10} Ω. The measured final insulation resistance in all the cases presents the same values. The resistance is measured every 30 minutes to verify that there is no unnoticed silver migration during the test. Furthermore, visual inspection shows that there are not dendrites or Ag growth at the end of the test.

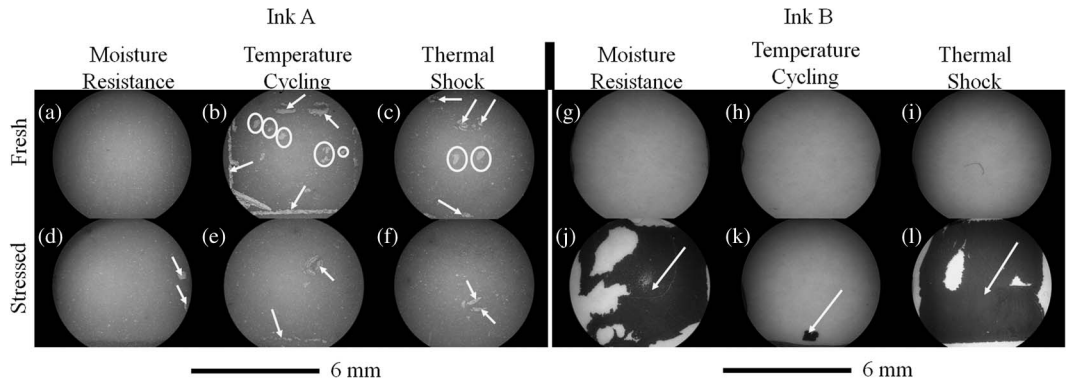

Fig. 7. Adhesion test results for (a)–(f) Ink A and (g)–(l) Ink B. Circles show adhesion failure occurring in the tape (desirable), and arrows show adhesion failure occurring in the ink (undesirable).

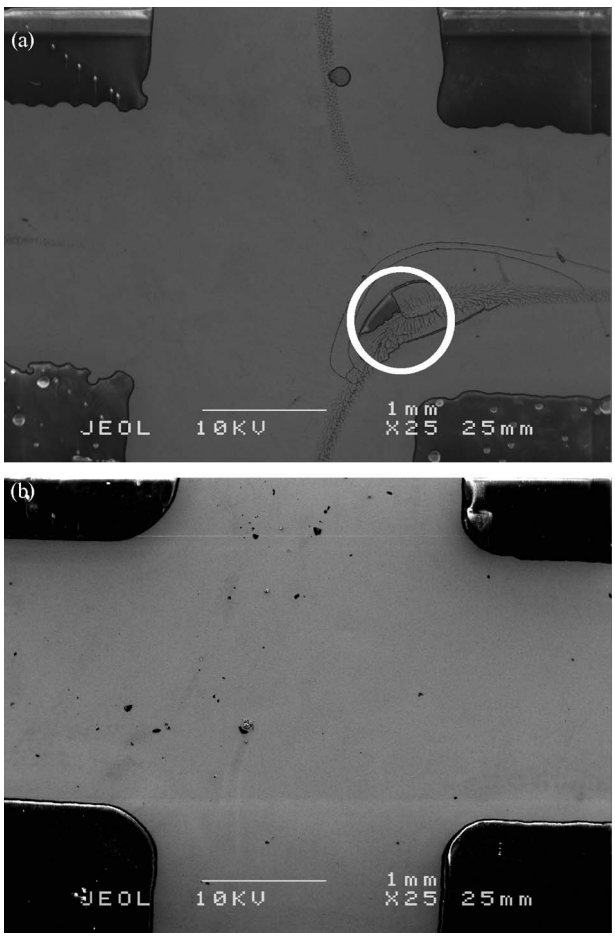

Fig. 8. Center of inkjet-printed structures with (a) Ink A and (b) Ink B with a magnification of 25×.

Failures during the THB test are required to determine the expected lifetime of the interconnections. Since there are no failures within the duration of the test, an expected life time is calculated using the acceleration factor formula in [19]. Such formula is expressed in (4) where T_1 and $RH_1\%$ are the temperature and relative humidity percentage at normal conditions (21 °C/50% RH); T_2 and $RH_2\%$ represent the testing conditions

$$AF = 10^{3040\left(\frac{1}{T_1}-\frac{1}{T_2}\right)+0.00019\left[(RH_2\%)^2-(RH_1\%)^2\right]}. \quad (4)$$

The acceleration factor for the lines with spacing of 260 μm in between, tested at 125 °C/85% RH, is 3978. This means that the tested samples can work for 108 years under normal conditions (21 °C/50% RH) without failing.

IV. Conclusion

Printed interconnection circuits directly on shapeable Li-ion batteries are promising given the fact that the silver ink structures printed on the battery's foil pass all the reliability tests. The silver ink resistivity values obtained are about 6 times higher than bulk silver resistivity. The electrical performance of the ink when exposed to high temperatures and a humid environment is good.

The surface of the battery's packaging foil is by nature hydrophobic, it is necessary to modify the substrate's surface morphology and chemical properties in order to achieve the most favorable adhesion between the substrate and the ink. A plasma treatment of O_2 at 100 W during 180 s is performed for this purpose; such treatment is selected as it gives the best adhesion results according to the experiments. The samples are cleaned with ethanol after the plasma treatment.

The adhesion between Ink A and the substrate exhibits sporadic failures. The adhesion of Ink B does not present failures at all under not very humid environments; nevertheless, it presents a considerable amount of failures under extremely humid environments and further tests are proposed to research this behavior.

The manufacturer-specified curing schedule of Ink A is 210 °C for 60 minutes; to avoid damage to the substrate, it can be cured for longer time at a temperature lower than 160 °C. A high temperature (210 °C) causes cracking of the structure and damages the battery's packaging foil but a lower temperature than specified compromises the reproducibility in the resistivity of the samples. The curing temperature of Ink B is 125 °C which avoids the presence of cracks in the printed structure and allows achieving a better reproducibility.

To avoid damage to the substrate and problems due to improper curing caused by the use of non recommended curing schedules, the use of an ink with a manufacturer-specified curing schedule of less than 155 °C is recommended, in this case Ink B. The interconnection lines should be printed on the foil prior to building the battery to avoid damage to the

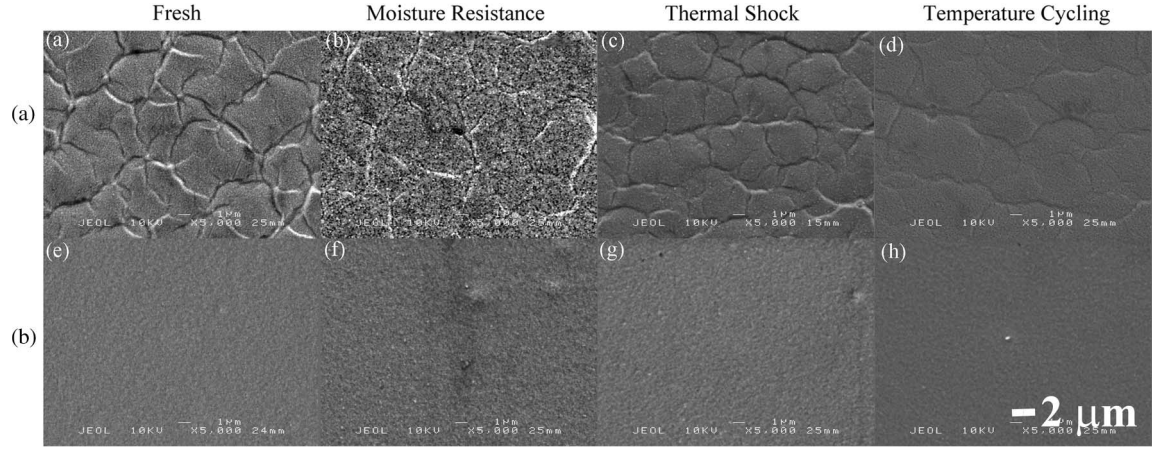

Fig. 9. Microstructure of both inks after all the aging processes.

electrolyte in the battery due to the curing temperature of the ink.

Ink B is the most suitable ink for printing the interconnections. Furthermore, Ink B presents no failures after the flexural testing and there is no presence of silver migration even when printing at the dimensional limits that the equipment and materials allow, under such dimensional limits, the devices have a life time of 108 years. Based on the experimental investigations detailed in this paper, it can also be concluded that the selected ink–substrate combination is suitable for practical applications.

For future research and ensuing applications, it is recommended low temperature (< 155 °C) curable inks or UV-curable inks. When using UV-curable inks, the interconnection circuits can be printed before or after forming the battery, as the user prefers.

In addition, it is possible to inkjet print the second level interconnects; electrically conductive adhesives are another possibility provided that aluminum is not the material in the contact pads due to known problems with its oxide layer. If components are soldered on to the interconnection lines, it is important that the molten solder does not affect the underlying interconnect; low temperature soldering materials (lower than 150 °C) are desired because of the restrictions of the battery's packaging foil. The techniques described in this paragraph would not affect the performance of the printed interconnects itself, however the compatibility of the materials to be used should be evaluated since it is not a widely used fabrication method. Furthermore, the temperature at which the second level interconnects are created will determine if this has to be done before or after forming the battery and injecting the electrolyte.

ACKNOWLEDGMENT

The authors would like to thank J. Bastemeijer, J. R. Mollinger, and Z.-Y. Chang for their valuable technical support, C.-K. Yang for the support with atomic force microscopy measurements, R. Poelma for the support with white light interferometry measurements, and, last but not least, the Delft Institute of Microsystems and Nanoelectronics staff members. The authors would also like to thank the people from Chemitox, Inc., for providing helpful information about what concerns the silver migration tests.

REFERENCES

[1] J. Zhou, "Lithium Metal Micro Reference Electrodes and Their Applications to Li-ion Batteries," Eindhoven Univ. Technol., Eindhoven, The Netherlands, 2007.

[2] A. Sridhar, D. J. van Dijk, and R. Akkerman, "Inkjet printing and adhesion characterization of conductive tracks on a commercial printed circuit board material," *Thin Solid Films*, vol. 517, no. 16, pp. 4633–4637, Jun. 2009.

[3] A. Sridhar, "An Inkjet Printing-Based Process Chain for Conductive Structures on PCB Materials," M.S. thesis, Univ. Twente, Enschede, The Netherlands, 2010.

[4] J. Perelaer, "Microstructures Prepared via Inkjet Printing and Embossing Techniques," Ph.D. dissertation, Eindhoven Univ. Technol., Eindhoven, The Netherlands, 2009.

[5] D. M. Svirachev and N. A. Tabaliov, "Plasma treatment of polymer surfaces in different gases," *Bulg. J. Phys.*, vol. 32, no. 1, pp. 22–23, 2005.

[6] N. Inagaki, S. Tasaka, K. Narushima, and H. Kobayashi, "Surface modification of PET films by pulsed argon plasma," *J. Appl. Polym. Sci.*, vol. 85, no. 14, pp. 2845–2852, Sep. 2002.

[7] A. Vesel and M. Mozetic, "Modification of PET surface by nitrogen plasma treatment," *J. Phys., Conf. Ser.*, vol. 100, no. 1, p. 012027, 2008.

[8] D. Papakonstantinou, E. Amanatides, D. Mataras, B. Ioannidis, and P. Nikolopoulos, "Improved surface energy analysis for plasma treated PET films," *Plasma Process. Polym.*, vol. 4, no. S1, pp. S1 057–S1 062, Apr. 2007.

[9] L. Jiangnan, B. Sunderland, J. Xue, S. Yan, W. Zhao, M. Folkard, B. D. Michael, and Y. Wang, "Study on hydrophobicity of polymer surfaces improved by plasma treatment," *Appl. Surf. Sci.*, vol. 252, no. 10, pp. 3375–3379, Mar. 2006.

[10] S. Enderling, C. L. Brown, III, S. Smith, M. H. Dicks, J. T. M. Stevenson, M. Mitkova, M. N. Kozicki, and A. J. Walton, "Sheet resistance measurement of non-standard cleanroom materials using suspended Greek cross test structures," *IEEE Trans. Semicond. Manuf.*, vol. 19, no. 1, pp. 2–9, Feb. 2006.

[11] M. G. Buehler, "An experimental study of various cross sheet resistor test structures," *J. Electrochem. Soc.*, vol. 125, no. 4, pp. 645–650, Apr. 1978.

[12] A. J. Walton, "Microelectronic test structures," in *Proc. SEMICOND.*, Geneva, Switzerland, 1997, pp. 1–10.

[13] L. J. van der Pauw, "A method of measuring specific resistivity and Hall effect of discs of arbitrary shape," *Philips Res. Rep.*, vol. 13, no. 1, pp. 1–9, Feb. 1958.

[14] N. B. Palacios Aguilera, U. Balda Irurzun, A. Sridhar, J. Bastemeijer, J. R. Mollinger, R. Akkerman, J. Zhou, P. J. French, and A. Bossche, "Shapeable Li-ion batteries as substrate: Printed electronics reliability," in *Proc. Int. Conf. Electron. Packag.*, Nara, Japan, Apr. 2011, pp. 844–848.

[15] A. Sridhar, M. Cauwe, H. Fledderus, R. H. L. Kuster, and J. Van Den Brand, "Novel interconnect methodologies for ultra-thin chips on foils," in *Proceedings of the ECTC*, San Diego, CA, 2012, pp. 238–244.

[16] Q. Wei, Y. Liu, D. Hou, and F. Huang, "Dynamic wetting behavior of plasma treated PET fibers," *J. Mater. Process. Technol.*, vol. 194, no. 1–3, pp. 89–92, Nov. 2007.
[17] "Polymer Thick Film—Material Performance and Reliability," Methuen, MA, Sep. 23, 2012.
[18] J. Liu, O. Salmela, J. Särkkä, J. Morris, P. Tegenhall, and C. Andersson, *Reliability of Microtechnology Interconnects, Devices and Systems*. New York: Springer-Verlag, 2011, p. 29.
[19] J. R. Dorfman, B. Schickling, and N. Metke, "Silver Migration-Resistant Polymer Thick Film Conductors for Appliance Circuitry," DuPont Micro-Circuit Mater., Research Triangle Park, NC, Sep. 23, 2012.

N. B. Palacios-Aguilera was born in Gómez Palacio, Durango, Mexico. She received the B.Sc. degree (with honors) in electronic systems engineering from Instituto Tecnológico y de Estudios Superiores de Monterrey (ITESM) Campus Laguna, Torreón, Mexico, in 2006 and the M.Sc. degree in electronic engineering with specialty in electronic systems from ITESM Campus Monterrey, Monterrey, Mexico, in 2008, where she worked in the design of a multiplexed potentiostat for activation of individually addressable microelectrode arrays in collaboration with the University of California, Irvine, a project sponsored by the University of California Institute for Mexico and the United States, Riverside. Since 2008, she has been working toward the Ph.D. degree in the Electronic Instrumentation Laboratory, Delft University of Technology, Delft, The Netherlands, working in low-temperature and low-cost packaging methods for system-in-package technology.

She has authored several conference papers and some journal papers.

Ms. Palacios-Aguilera was a recipient of the "Best Paper Award" at the Fifth International Conference on Quantum Nano and Micro Technologies in 2011.

H. A. Visser received the Ph.D. degree from the University of Twente, Enschede, The Netherlands, and the Eindhoven University of Technology, Eindhoven, The Netherlands, where he carried out a Ph.D. research project and successfully defended his Ph.D. thesis entitled "Residual lifetime assessment of PVC gas pipes" in 2010.

After a half year research project on tensile impact properties of polymers at Politecnico di Milano, Milano, Italy, he started working as an Assistant Professor with the Production Technology group, Faculty of Engineering Technology, University of Twente, where he is involved on research activities on inkjet printing and polymer mechanics.

Ashok Sridhar received the B.S. degree in mechanical engineering from the University of Madras, Chennai, India, in 2001, the M.S. degree in production engineering from the Aachen University of Technology (RWTH), Aachen, Germany, in 2006, and the Ph.D. degree from the University of Twente, Enschede, The Netherlands, in 2010, for the development of an inkjet-printing-based process chain to fabricate conductive circuit structures on printed circuit board materials. He has authored several journal papers and contributed to several conferences. Since May 2011, he has been a Researcher with the TNO/Holst Centre, Eindhoven, The Netherlands, specializing in ultrathin chip integration and interconnection technologies for systems in foil.

Dr. Sridhar was a recipient of the "Best Poster Award" and the "Best Author Award" at the Printing Future Days Conferences in 2007 and 2009, respectively.

Unai Balda-Irurzun received the B.Sc. degree in industrial design engineering from the University of Mondragon, Mondragon, Spain, in 2008 and the M.Sc. degree in emerging technologies design from the University of Twente, Enschede, The Netherlands, in 2010.

He was a Project Manager with CAF, S.A., Beasain, Spain, working on high-speed train's axle protection systems and an R&D engineer with Fagor Electrónica, Mondragon. He is currently a High-Precision Engineer with Innovalia Metrology, Bilbao, Spain.

Laura D. Vargas-Llona was born in Oviedo, Spain. She received the B.S. degree in physics from the University of Cantabria, Santander, Spain, in 1995.

Since then, she has been with the University of Twente, Enschede, The Netherlands, where she worked in several different groups on themes in superconducting electronics and nickel electroplating for micromechanical devices and is currently a Microscopist for materials analysis in the Production Technology group.

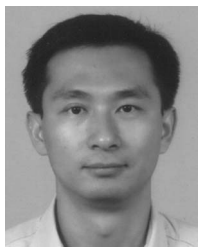

Jiang Zhou was born in Shangrao, Jiangxi, China. He received the B.S. degree in electrochemistry from the Department of Applied Chemistry, Tianjin University, Tianjin, China, in 1992 and the M.Eng. degree with a thesis on the topic of catalytic removal of pyridine from the National University of Singapore, Singapore, in 2002. He is currently working toward the Ph.D. degree at the Eindhoven University of Technology (Inorganic Chemistry and Catalysis group), Eindhoven, The Netherlands, where his research was focused on the development of lithium metal microreference electrodes in order to carry out *in situ* electrochemical characterization of Li-ion batteries. His work was performed in the System-in-Package Devices group, Philips Research Europe, Eindhoven.

In 1996, he joined HuaFei Color Display System Company, Ltd., as a Process Engineer. In 1997, he performed a traineeship at Philips in France, The Netherlands, and Germany. In 2006, he joined System-in-Package Devices group, Philips Research Europe, as a Research Scientist.

Remko Akkerman received the Ph.D. degree with a thesis on viscoelastic flow simulations from the University of Twente, Enschede, The Netherlands, in 1993.

He was appointed Full Professor in production technology in 2003. Since 2009, he has been the Scientific Director of the ThermoPlastic Composite Research Centre, Enschede. His research focus is on composite materials, ranging from efficient processing to performance optimization and functional materials.

P. J. French was born in Rochford, U.K. He received the B.Sc. degree in mathematics, the M.Sc. degree in electronics, and the Ph.D. degree with a thesis study on the piezoresistive effect in polysilicon from the University of Southampton, Southampton, U.K., in 1981, 1982, and 1986, respectively.

He then spent 18 months with Delft University of Technology, Delft, The Netherlands, on the Royal Society European Exchange Programme, investigating new flip-flop sensor structures. In 1988, he was with the Central Engineering Laboratories, Nissan Motor Company, Japan, working on sensors for automotive applications. In 1991, he began a three-year FOM sponsored fellowship with the Electronic Instrumentation Laboratory, Delft University of Technology, to study micromachining, where he became the Head in 2002 and has been one of the project leaders since 1994. In 1999, he was appointed as the Antoni van Leeuwenhoek Chair. His main research interests are silicon technology, mechanical sensors and actuators, MOS-based sensors, and process optimization related to sensors.

Andre Bossche was born in Rotterdam, The Netherlands, in 1956. He received the M.Sc. (with honors) and Ph.D. degrees in electrical engineering from Delft University of Technology, Delft, The Netherlands, in 1983 and 1988, respectively.

He is an Associate Professor with the Department of Microelectronics, Delft University of Technology, where he is the Leader of the Biodevices Research Group, Electronic Instrumentation Laboratory, Delft Institute of Micro-Electronics and Submicron Technology. He is the author or a coauthor of two books and more than 180 scientific papers in journals and conference proceedings. His project group is engaged in research work on the subjects of the following: reliability of integrated sensors and MEMS devices (in particular, the reliability of microstructures and materials), micro- and nanofluidic devices for biochemical analysis, sensors, and microsystems for medical applications.